

# Chapter 7

## Stress–Strain and Fluid Flow



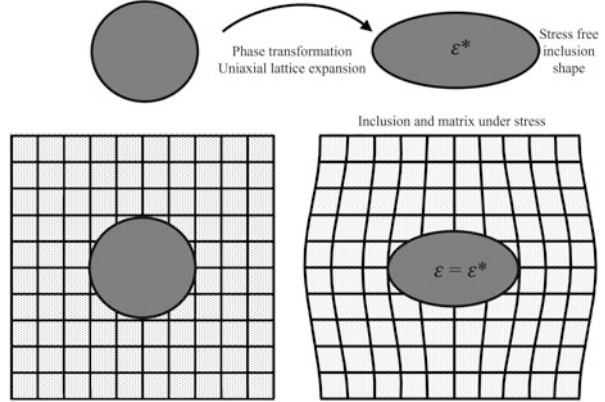
### 7.1 Coupling to Stress and Strain

In this last lecture, before we change gears to the “quantum-phase-field” model, we want to (almost) complete the picture of the effects to be considered in real materials. “Almost,” because we discuss only elasticity and fluid flow; we only touch on plasticity, and we neglect electric charges, magnetic coupling, and others. As stated in Chap. 1, a wide range of applications of phase-field modelling and simulations lies in this field. The models applied there, however, are complementary in concept with what we will discuss now: coupling of phase evolution with elastic distortion.

It is reported that Armen Khachaturyan developed his branch of phase fields, the so-called “time-dependent Ginsburg–Landau theory,” to predict the equilibrium shape of a martensite needle in parent austenite. The problem relates to the old Eshelby problem of an inclusion in a matrix with finite transformation strain [9]. We may also include deviatoric strain if the crystal lattice changes from BCC to FCC. This was used to find the solution to the problem of the equilibrium shape of a crystal in its melt using the anisotropy of the interface energy in Chap. 3. Practically speaking, and this is often reported in the literature (to which I give no reference here), you cut out a piece of material from a crystal, transform it to a different phase with volumetric and deviatoric distortion with respect to the original crystal, and put it back. Continuity demands that both the parent and child crystal have to deform elastically to form a common body (see Fig. 7.1).

In the phase-field approach, this is an easy exercise: you simply have to add the elastic bulk free energy of the individual phases to our previous models and decide on a good way to handle the elastic contribution within the interface. The elastic bulk free energy  $f^{\text{elast}}$  is (and all phase-field models agree with classical models from continuum mechanics on this point):

**Fig. 7.1** Scheme of the elastic equilibrium between a transformed inclusion and the matrix



$$f^{\text{elast}} = \frac{1}{2} \left\{ \sum_{\alpha=1}^{\tilde{N}} \phi_{\alpha} (\epsilon_{\alpha}^{ij} - \epsilon_{\alpha}^{*ij}) C_{\alpha}^{ijkl} (\epsilon_{\alpha}^{kl} - \epsilon_{\alpha}^{*kl}) \right\}, \quad (7.1)$$

where  $\epsilon_{\alpha}^{ij}$  is the total strain in phase  $\alpha$ ,  $\epsilon_{\alpha}^{*ij}$  is the eigenstrain (or transformation free strain), and  $C_{\alpha}^{ijkl}$  is the elasticity matrix. We use the sum convention for double indices.

In general,  $\epsilon_{\alpha}^{*ij}$  and  $C_{\alpha}^{ijkl}$  are concentration- and temperature-dependent quantities, which gives rise to intriguing effects of chemo-mechanical coupling (see [16] and references therein). We leave this for further reading. The ansatz (7.1) is a direct extension of the original multi-phase model for diffusive phase transformations, as the total elastic energy is a linear summation of the elastic energies of the individual phases weighted by the phase densities  $\phi_{\alpha}$ . It is mostly assumed that the equilibrium is instantaneous. One derives the mechanical equilibrium equation, as we do with all relevant transport equations, as a functional derivative from the free-energy functional

$$\vec{0} = \nabla \sigma = \nabla \frac{\delta}{\delta \epsilon} F \quad (7.2)$$

in vector notation, where the stress  $\sigma$  and strain  $\epsilon$  are rank-two tensors. The difficulty now is to define these tensors within the interface, because the definition of the elastic free energy density (7.1) uses different strains  $\epsilon_{\alpha}$ . In all bulk phases, the stress is of course  $\sigma = \epsilon C$ , but also the elasticity  $C$  is only defined for each phase. This is a classical problem in solid mechanics: to define an effective material from a mixture of materials, so-called mathematical homogenization. To be able to solve the mechanical equilibrium equation (7.2), one first has to define the effective mechanical properties of the interface, the effective elasticity matrix  $C$ , and also the effective transformation strain  $\epsilon^*$ . The latter is commonly taken as a weighted average  $\epsilon^* = \sum_{\alpha} \phi_{\alpha} \epsilon_{\alpha}^*$ . In the phase-field literature, the most-used homogenization

for the total strain tensor  $\epsilon$  is the so-called Voigt–Taylor model, which assumes homogeneous strain in all phases  $\epsilon = \epsilon_\alpha = \epsilon_\beta$ . Then, however, the stress has to be discontinuous in general. The opposite, the Reuss–Sachs model, takes the stress as continuous between the phases. Since the stress is the equivalent to a chemical potential in a mechanical system, one may take this assumption as an analogue to equal chemical potential in the interface (see also the discussion in [20]).

A combination of both models, taking the strain as continuous in the tangential direction and the stress as continuous in the normal direction to the interface, is proposed in [8]. The most advanced model is the so-called rank-one convexification applying a jump condition (see [15, 17]). We leave this topic to further reading. Only one important consequence shall be detailed here: the elastic driving force for phase transformations  $\Delta g_{\alpha\beta}^{\text{elast}}$  for a phase-transformation under mechanical load, either external or by internal stresses. For the Voigt–Taylor model, we find for the dual  $\alpha$ – $\beta$  interface (the general form is defined as a superposition between dual driving forces in the multi-phase-field approach):

$$\begin{aligned}\Delta g_{\alpha\beta}^{\text{elast}} &= \left( \frac{\delta}{\delta\phi_\alpha} - \frac{\delta}{\delta\phi_\beta} \right) F \\ &= (\epsilon_\alpha^* - \epsilon_\beta^*)(\epsilon - \epsilon^*)C + \frac{1}{2}(\epsilon - \epsilon^*)^2(C_\alpha - C_\beta).\end{aligned}\quad (7.3)$$

For Reuss–Sachs, we have:

$$\Delta g^{\text{elast}} = (\epsilon - \epsilon^*)C(\epsilon_\alpha^* - \epsilon_\beta^*)C \left[ (\epsilon_\alpha^* - \epsilon_\beta^*) - \frac{1}{2} \left( \frac{1}{C_\alpha} - \frac{1}{C_\beta} \right) C(\epsilon - \epsilon^*) \right]. \quad (7.4)$$

We see in both cases, that the elastic driving force for phase transformations vanishes for a homogeneous material if  $\epsilon_\alpha^* = \epsilon_\beta^*$  AND  $C_\alpha = C_\beta$ . Also in both cases we have two contributions: one related to the difference in the eigenstrains, the other related to the difference in the elasticity matrices. And of course, the elastic driving force vanishes if the total strain matches the eigenstrains, i.e., there is no stress in the interface region. Higher-order schemes considering a jump condition between stress and displacement at the interface [8, 15, 17] are more involved, but they follow the same principles.

Another remark relates to the solution of the mechanical equilibrium equation (7.2). This can be achieved by any appropriate numerical approach using a finite-element scheme in real space. In phase-field models, the Fourier method is very popular because its solution for homogeneous systems, i.e.,  $C = C_\alpha = C_\beta$ , is computationally very cheap. If the material cannot be approximated by homogeneous elasticity, one first solves a homogeneous problem and then corrects the solution for the inhomogeneity in an iterative scheme. The difference between the elasticity coefficients is called “contrast.” In the case of a low contrast, i.e., if the elasticity in all phases is similar, these schemes are quite effective. For high contrast, e.g., a pore filled with gas or liquid in a solid metal, one needs more elaborate schemes [12].

One also has to consider that the Fourier transformation relies on periodic boundary conditions. In any case, however, one should not confuse the theoretical setup of the phase-field model with a special solution procedure, as important as this is for application.

The final comment regards plasticity. There may be an outer load that exceeds the yield point of the material. Then, elastic strain is limited, and plastic strain sets in. This is associated with dislocation activity and the generation of another contribution to the free energy of the system: stored plastic energy related to dislocations. Such stored plastic energy may lead to phenomena such as “recrystallization.” This can be treated similarly to a phase transformation, and it is driven by the reduction of plastic energy. This is “easy” from a phase-field perspective, but it is difficult in terms of handling plastic energy at the continuum scale. It is even more difficult to design a model accounting for how moving interfaces interact with dislocations. Some applications are suggested for further reading. Additionally, internal stresses, which are caused by transformation strain between different phases, may exceed the yield point of the material, in particular at elevated temperatures. The stress state of the interface, and thus the driving force for phase transformation, is then limited by plastic relaxation. Therefore, plasticity will generate new driving forces on the one hand, and it will reduce driving forces on the other hand. This is a wide area for future research, but it is associated with special challenges regarding (i) model formulation and (ii) numerical solution.

### **Example—Martensitic Transformation**

A body-centered-tetragonal martensite structure is formed by rapidly quenching from the face-centered-cubic austenite phase. When a material undergoes a martensitic transformation, the crystalline unit cell undergoes a shape change. The final microstructure of martensite is strongly influenced by elastic energy generated during the change of the crystal structure. Accommodation of the elastic energy is often achieved by forming a multi-variant domain. In addition, plastic deformation occurs in the austenite matrix and the growing martensite phase, and these are called self-accommodation and plastic accommodation, respectively [5, 23]. Thus, both elastic and plastic effects play important roles in martensitic transformations.

### **The Simulation**

A 3D multi-phase-field model was used to model martensite microstructure formation in low-carbon steel. In this example (Fig. 7.2), an elasto-plastic approach is employed with a full set of 24 Kurdjumov–Sachs symmetry variants of martensite with real transformation strains [13]. A finite strain

(continued)

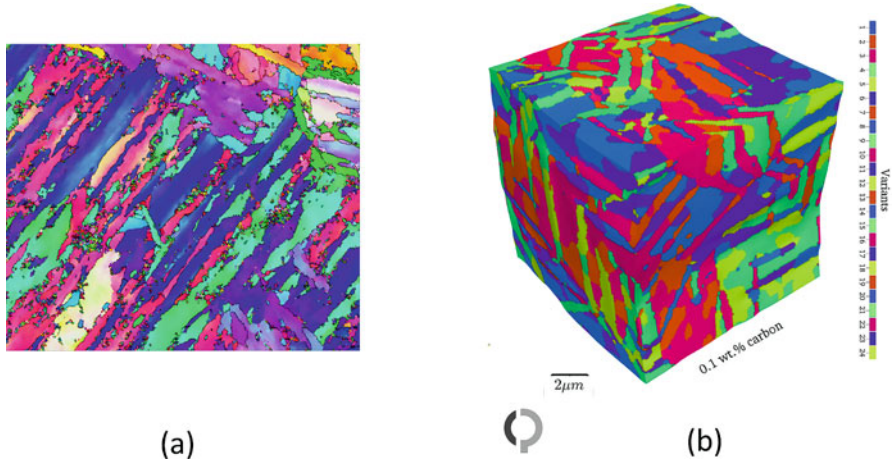


**Fig. 7.2** Lath martensite microstructures: (a) electron backscatter diffraction map of martensite in a sample containing 0.1 wt.% carbon [18]; and (b) simulated martensite microstructure in low-carbon steel consisting of 24 Kurdjumov–Sachs symmetry variants, indicated by color coding

framework is applied in connection to a phenomenological crystal-plasticity model. Both methods are fully coupled within the **OpenPhase** library.

## 7.2 Coupling to Fluid Flow

In previous lectures, we have discussed the coupling of the phase field with temperature, solute, and elastic distortion. In all these cases, the driving force for a phase transformation  $\Delta g_{\alpha\beta} = \left( \frac{\delta}{\delta\phi_\alpha} - \frac{\delta}{\delta\phi_\beta} \right) F$  is directly dependent on temperature, composition, or stress. We consider this coupling as “strong.” In the present subsection, we consider fluid flow, or melt flow when considering a solidification process. The coupling to phase evolution may be considered as “weak,” since the direct effect of flow on a phase transformation, the Clausius–Clapeyron effect, is generally very weak. The Clausius–Clapeyron effect describes the boiling temperature of a liquid dependent on the pressure in the system: the boiling temperature of water is significantly reduced on high mountains. The melting temperature of a metal, however, is hardly affected by the pressure of a streaming melt, and we therefore simply neglect it. There is, however, a strong effect of melt flow on dendrite morphologies in solidification. This is because on the one hand, melt flow significantly affects the transport of solute and heat in the melt; on the other hand, solidification significantly affects the viscosity of the material.

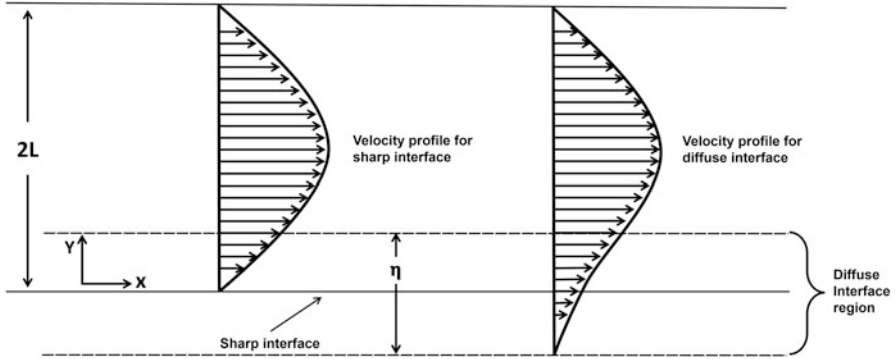


**Fig. 7.3** Schematic of channel flow in which the width of the channel and the width of the interface are of the same order of magnitude

A solid dendrite can be seen as a rigid body. If it is attached to the mold of the casting, it forms a rigid barrier for flow; if it is transported with the melt as an equiaxed crystal, it will affect the effective viscosity of the two-phase system (solid and melt). If the solid fraction is low, a metallic melt has a viscosity like that of water; if the solid fraction exceeds 30%, it will behave like honey with precipitated sugar crystals; above 50%, any melt flow will stop.

This mutual interaction leads to intriguing phenomena, which we will leave for further reading. Here, we will elaborate on one effect that is crucial for the interaction of a fluid with a solid when the interface between liquid and solid is diffuse at a mesoscopic scale. At the microscopic scale, we definitely accept a so-called “no-slip” condition: the flow velocity decays to 0 monotonously in the direction normal to the interface. Figure 7.3 schematically shows the condition of a channel flow in which the width of the channel and the width of the interface are of the same order of magnitude. One side of the channel is treated as a “wall,” i.e., a sharp interface with a well-defined no-slip condition; the other side is treated as diffuse in the context of phase-field theory. How do we realize an analogue to the no-slip condition within a diffuse boundary? As in the first part of this lecture, we treat the interface as an effective material, and in the present case as a porous medium: the flow will penetrate the interface, but the permeability of the interface will be a function of the phase field.

The corresponding fluid-flow equation for the fluid velocity  $\vec{u}$  in a mixed domain—solid and liquid—is readily written down (for simplicity, without moving solids, i.e., the solid velocity is set to 0;  $\phi = \phi_{\text{liquid}}$ , density  $\rho$  set to 1):

$$\frac{\partial}{\partial t} \phi \vec{u} + \vec{\nabla} \phi \vec{u} \vec{u} = -\phi \vec{\nabla} P + \vec{\nabla} (\nu \nabla \phi \vec{u}) - h^* X_l. \tag{7.5}$$

The important part here is the last term: friction within the diffuse interface  $X_I$ . This has been worked out for the planar interface with a friction coefficient  $h^*$ .<sup>1</sup> Its numerical value is given as  $h^* = 2.757$  [6]. Other models defining the no-slip condition as a function of the phase field have been investigated [3, 4, 21] and may be investigated in the future. A consistent investigation for curved interfaces (concave or convex) is still missing. In any case, we will require the “sharp-interface solution” to be met outside of the interface, i.e., that we meet the sharp-interface model in the bulk. In the case of the channel flow, the sharp-interface model predicts a parabolic velocity profile in the channel: Hagen–Poiseuille law. The maximum velocity is a sensitive indicator of whether the diffuse interface correctly emulates the sharp interface; it is a kind of “thin-interface limit,” i.e., we match a sharp-interface solution in the bulk liquid but deviate systematically within the thin interface.

## 7.3 Exercises

### Exercise

Derive the expressions for the elastic driving forces (7.3) and (7.4) for the Voigt–Taylor and Reuss–Sachs limit, respectively.

### Example: Dendritic Solidification Interacting with Shear Flow of the Melt

The setup (Fig. 7.4) represents a thin Mg–Al melt channel between two rigid walls. We see nucleation and growth of  $\alpha$ -Mg dendrites. At the same time, shear flow is introduced to the melt via the motion of the rigid walls. Full integration of the inertial and friction forces acting on the solid dendrites and the melt results in the dendrites moving with the melt. In this example, the fluid-flow problem is solved using the lattice Boltzmann method, while the system morphology and its evolution is described by the phase-field method. Both methods are fully coupled within the **OpenPhase** library, allowing the study of arbitrarily complex geometries. See [14, 22].

---

<sup>1</sup>  $h^*$  is named the “Hermann-Joseph” constant. Hermann-Joseph Diepers was one of my early collaborators. He passed away from cancer before finishing his PhD. His memory lasts.

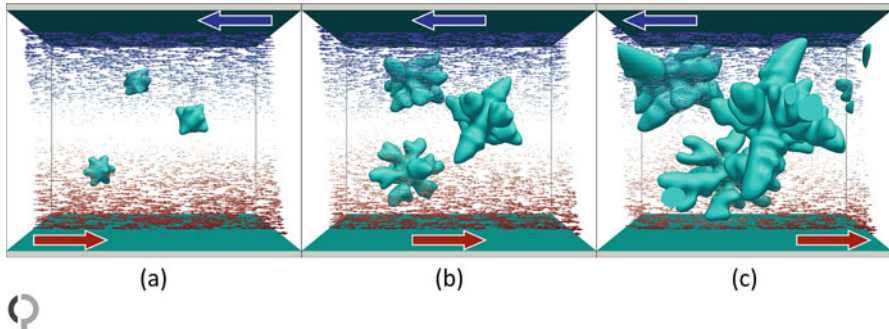


**Fig. 7.4** Flow simulation of Mg–Al alloy solidification

### Further Reading

- Chemo-mechanical coupling [10, 16].
- Hadamard jump [15, 17].
- Recrystallization and rafting under high-temperature creep [1, 2, 7, 11].
- Dendritic growth with buoyancy [19, 22].

### References

1. M. Ali, et al., 45-degree rafting in Ni-based superalloys: a combined phase-field and strain gradient crystal plasticity study. *Int. J. Plast.* **128**, 102659 (2020). <https://doi.org/10.1016/j.ijplas.2020.102659>
2. M. Ali, J.V. Görler, I. Steinbach, Role of coherency loss on rafting behavior of Ni-based superalloys. *Comput. Mater. Sci.* **171**, 109279 (2020). <https://doi.org/10.1016/j.commatsci.2019.109279>
3. D.M. Anderson, G.B. McFadden, A.A. Wheeler, A phase-field model of solidification with convection. *Physica D* **135**, 175–194 (2000)
4. D.M. Anderson, G.B. McFadden, A.A. Wheeler, A phase-field model of solidification with convection: sharp-interface asymptotics. *Physica D* **151**, 305–331 (2001)
5. G.R. Barsh, et al., A new view on martensitic transformations. *Scripta Metallurgica* **21**(9), 1257–1262 (1987)
6. C. Beckermann, et al., Modeling melt convection in phase-field simulations of solidification. *J. Comput. Phys.* **154**, 468–496 (1999)
7. S. Chakraborty, et al., Investigating the origin of cube texture during static recrystallization of FCC metals: a full field crystal plasticity-phase field study. arXiv: 2006.06475 [cond-mat.mtrl-sci] (2020)
8. A. Durga, P. Wollants, N. Moelans, A quantitative phase-field model for two-phase elastically inhomogeneous systems. *Comput. Mater. Sci.* **99**, 81–95 (2015). <https://doi.org/10.1016/j.commatsci.2014.11.057>
9. J.D. Eshelby, The elastic field outside an ellipsoidal inclusion. *Proc. R. Soc. Lond. A* **252**, 561–569 (1959). <https://doi.org/10.1098/rspa.1959.0173>

10. J. Görler, et al., Gamma-channel stabilization mechanism in Ni-base superalloys. *Philos. Mag. Lett.* **95**(11), 519–525 (2015). <https://doi.org/10.1080/09500839.2015.1109716>
11. J. Hiebeler, et al., Modelling of flow behaviour and dynamic recrystallization during hot deformation of MS-W 1200 using the phase field framework, in *MATEC Web of Conferences*. EDP Sciences, vol. 80 (2016), p. 01003. <https://doi.org/10.1051/mateconf/20168001003>
12. S.Y. Hu, L.Q. Chen, A phase-field model for evolving microstructures with strong elastic inhomogeneity. *Acta Mater.* **49**(11), 1879–1890 (2001). [https://doi.org/10.1016/s1359-6454\(01\)00118-5](https://doi.org/10.1016/s1359-6454(01)00118-5)
13. G. Kurdjumow, G. Sachs, Über den mechanismus der stahlhärtung. *Z. Phys.* **64**(5–6), 325–343 (1930)
14. D. Medvedev, F. Varnik, I. Steinbach, Simulating mobile dendrites in a flow. *Proc. Comput. Sci.* **18**, 2512–2520 (2013)
15. J. Mosler, O. Shchyglo, H. Montazer Hojjat, A novel homogenization method for phase field approaches based on partial rank-one relaxation. *J. Mech. Phys. Solids* **68**, 251–266 (2014). <https://doi.org/10.1016/j.jmps.2014.04.002>
16. J. Park, et al., First evidence for mechanism of inverse ripening from in-situ TEM and phase-field study of  $\delta'$  precipitation in an Al–Li alloy. *Sci. Rep.* **9**, 3981 (2019). <https://doi.org/10.1038/s41598-019-40685-5>
17. D. Schneider, et al., Phase-field elasticity model based on mechanical jump conditions. *Comput. Mech.* **55**(5), 887–901 (2015). <https://doi.org/10.1007/s00466-015-1141-6>
18. O. Shchyglo, et al., Phase-field simulation of martensite microstructure in low-carbon steel. *Acta Mater.* **175**, 415–425 (2019)
19. I. Steinbach, Pattern formation in constrained dendritic growth with solutal buoyancy. *Acta Mater.* **57**, 2640–2645 (2009). <https://doi.org/10.1016/j.actamat.2009.02.004>
20. I. Steinbach, M. Apel, Multi phase field model for solid state transformation with elastic strain. *Physica D* **217**, 153–160 (2006). <https://doi.org/10.1016/j.physd.2006.04.001>
21. A. Subhedar, I. Steinbach, F. Varnik, Modeling the flow in diffuse interface methods of solidification. *Phys. Rev. E* **92**(2), 023303 (2015). <https://doi.org/10.1103/PhysRevE.92.023303>
22. M. Tegeler, et al., Effect of microstructure during dendritic solidification on melt flow: a phase-field lattice-Boltzmann study, in *Proceedings of the 6th Decennial International Conference on Solidification Processing* (2017)
23. A. Yamanaka, T. Takaki, Y. Tomita, Elastoplastic phase-field simulation of self-and plastic accommodations in cubic  $\rightarrow$  tetragonal martensitic transformation. *Mater. Sci. Eng. A* **491**(1–2), 378–384 (2008)

**Open Access** This chapter is licensed under the terms of the Creative Commons Attribution 4.0 International License (<http://creativecommons.org/licenses/by/4.0/>), which permits use, sharing, adaptation, distribution and reproduction in any medium or format, as long as you give appropriate credit to the original author(s) and the source, provide a link to the Creative Commons license and indicate if changes were made.

The images or other third party material in this chapter are included in the chapter's Creative Commons license, unless indicated otherwise in a credit line to the material. If material is not included in the chapter's Creative Commons license and your intended use is not permitted by statutory regulation or exceeds the permitted use, you will need to obtain permission directly from the copyright holder.

